ELSEVIER

Journal of Power Sources 81–82 (1999) 73–78

JOURNAL OF POWER SOURCES

www.elsevier.com/locate/jpowsour

# Jahn–Teller instability in spinel Li–Mn–O

Atsuo Yamada *, Masahiro Tanaka, Koichi Tanaka, Koji Sekai

*Research Center, Sony Corporation, 174 Fujutsuka-cho, Hodogaya-ku, Yokohama 240, Japan*

**Abstract**

Various compositions in the spinel Li–Mn–O system were prepared and characterized by thermal analysis, X-ray diffraction, and X-ray absorption spectroscopy, with special attention to the Jahn–Teller (JT) instability of $Mn^{3+}$. Of particular interest are (1) the discovery of JT structural phase transitions around 280 K, demonstrating that $LiMn_2O_4$ involves large JT instability in spite of its cubic symmetry at room temperature, (2) the use of transition temperature, $T_t$, and latent heat, $\Delta H$, as sensitive parameters of JT instability in the practical composition region of the spinel Li–Mn–O ternary system as a 4 V cathode, and (3) the identification of the large, non-cooperative local JT distortion around $Mn^{3+}$ in the cubic phase. 

*Keywords:* Lithium-ion batteries; Cathodes; Lithium manganese oxides; Jahn–Teller effect; Local structure; EXAFS

## 1. Introduction

Recently, much attention has been focused on lithiated manganese oxides as candidates to replace expensive $LiCoO_2$ in cathodes, especially for large-scale rechargeable lithium ion batteries, where the cost of unit weight/volume is a crucial factor. In particular, low-cost lithium-ion batteries for electric vehicles would encourage development of a more environment-friendly society.

Among the large family of Li–Mn–O compounds, $LiMn_2O_4$-based materials with a spinel structure (cubic space group Fd3m) are of technical interest because they provide a large number of tetrahedral 8a sites for mobile lithium ions within the $Mn^{4+/3+}$ redox couple and hence have large electrochemical capacity in the 4 V region [1]. Although $LiMn_2O_4$ spinels are now about to be commercialized, metastable polymorphs of $LiMnO_2$ with various space groups, e.g., Pmnm [2], C2/m [3], R3m [4], and amorphous forms of lithiated manganese oxides [5] are being studied as alternatives.

It is important to note, however, that all Li–Mn–O cathodes using the $Mn^{4+/3+}$ redox couple suffer from large Jahn–Teller (JT) instability caused by trivalent manganese ions (electron configuration: $t_{2g}^3e_g^1$) at the octahedral sites. JT instability is a potential negative characteristic of battery cathodes and deserves careful investigation. The anisotropic volume change on passing through the cubic-tetragonal transition leads to a loss of electrode-storage capacity on repeated discharge/recharge cycling [6]. The instability is especially enhanced in a nonequilibrium discharge condition which forms the $Mn^{3+}$-rich region at the surface of the electrode [7].

In trivalent manganospinels, e.g., $MgMn_2O_4$ and $ZnMn_2O_4$, a cooperative JT transition from cubic (Fd3m) to tetragonal ($I4_1/amd$) takes place at temperature $T_t \sim$ 1400 K and the tetragonal distortion ($c/a$) is as large as 1.15 at room temperature [8]. The transition temperature $T_t$ and the distortion $c/a$ have a moderate correlation to the electronic structure of the $MnO_6^{9-}(Mn^{3+})$ octahedron in the ground state because of the thermal excitation of electrons over the energy gap $\Delta$ ($d_{z^2}$ to $d_{x^2-y^2}$ orbital in tetragonal $D_{4h}$ symmetry), $\Delta \sim k_B T_t \propto (c/a - 1)$ [9], i.e., $\Delta/k_B$ is approximately $\sim$1400 K (see Fig. 1).

The replacement of the trivalent manganese ions by divalent ($t_{2g}^3e_g^2$) or tetravalent ($t_{2g}^3e_g^0$) manganese ions reduces the instability. Consequently, $T_t$ decreases and the magnitude of $c/a$ decreases and approaches unity as the average manganese valence number increases from $v = +3.0$ to $v = +3.5$ [10–12]. In the lithium manganospinel system, $LiMn_2O_4$ is of particular interest because it takes the threshold manganese valence, $v = +3.5$, where the cubic lattice is apt to exhibit JT distortion when the manganese valence is slightly reduced by lithium insertion [13] or oxygen extraction [10,14,15].

This situation led us some years ago to an investigation of the low temperature structure of $LiMn_2O_4$ and the discovery of the unique cubic-tetragonal transition in the

* Corresponding author. Tel.: +81-45-353-6857; Fax: +81-45-353-6910; E-mail: ayamada@src.sony.co.jp

0378-7753/99/$ - see front matter 
PII: S0378-7753(99)00106-8

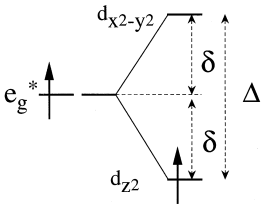


Fig. 1. Electronic structure of $Mn^{3+}$ in oxygen octahedra.

vicinity of $T_t = 280$ K [11]. Previously published work done at the Sony Research Center exploring this topic [9–12,16,17] is reviewed in this paper. The large local JT distortion around $Mn^{3+}$ in the cubic phase will also be discussed in analogy with the $La_{1-x}A_xMnO_3$ (A = Sr, Ca, Pb) perovskite system.

## 2. Experimental

### 2.1. Materials synthesis

The $LiMn_2O_4$ sample was prepared by reacting $Li_2CO_3$ and $Mn_2O_3$. The starting materials, $Li_2CO_3$ (4 N) and $Mn_2O_3$ (3 N) powders, were coarsely mixed at a 1:2 Li:Mn ratio and ball-milled for about 24 h in ethanol. After evaporating the ethanol at 70°C, the samples were reground and calcined at 750°C in air, after which they were fired at 870°C in $O_2$ for 24 h and slowly cooled to room temperature. The $LiMn_2O_4$ obtained and $Li_2CO_3$ were mixed in various molar ratios to form $Li(Li_xMn_{2-x})O_4$ and calcined at 650°C in $O_2$ for 15 h. λ-$MnO_2$ was prepared by conversion from $LiMn_2O_4$. $LiMn_2O_4$ in a HCl solution was stirred for 3 h. The solution was then decanted and the remaining solid materials were washed, filtered in a sintered glass filter, and dried in vacuum. $ZnMn_2O_4$ was synthesized by a solid-state reaction. The stoichiometric mixture of ZnO and $MnCO_3$ was ball-milled with ethanol for 12 h, calcined at 700°C for 10 h, then sintered at 900°C for 20 h. The composition and crystal structure were confirmed by inductively coupled plasma (ICP) emission spectroscopy and X-ray diffraction analysis.

### 2.2. Characterization

The characteristics of $LiMn_2O_4$ after oxygen extraction at elevated temperatures and their dependence on the oxygen partial pressure were investigated using thermogravimetric and differential thermal analysis (TG/DTA, Shinku-Rico, TGD-7000) in various atmospheres. The sample was 200 mg of $LiMn_2O_4$ powder. The standard sample used for DTA measurements is 200 mg of α-$Al_2O_3$ (5 N). The partial pressure, $P_{O2}$, was controlled from 0 to 1 atm by changing the $O_2/N_2$ ratio. The flow rate of the mixed gas was 50 $cm^3$/min.

Differential scanning calorimetric (DSC) measurements were performed at a rate of 5 K/min in the temperature range between 150 K and 400 K to detect the phase transitions in $Li(Li_xMn_{2-x})O_4$. The 50 mg samples of $Li(Li_xMn_{2-x})O_4$ and α-$Al_2O_3$ with 99.999% purity were packed into small aluminum cells and were set in the measuring apparatus (Shinku-Riko, DSC-7000). The measurements were performed in dry nitrogen at a pressure of 500 mmHg.

The temperature dependence of the powder X-ray diffraction pattern for $LiMn_2O_4$ was recorded in a dry nitrogen flow from 220 K to room temperature with an automated Rigaku diffractometer and CuKα radiation. The temperature of the sample was held constant during the measurements and was controlled by balancing the liquid nitrogen flow and the heat.

X-ray absorption measurements were performed for $LiMn_2O_4$, using λ-$MnO_2$ and $ZnMn_2O_4$ as reference samples, at beam line BL-10B in the Photon Factory of the National Laboratory for High Energy Physics (KEK) in Tsukuba, Japan, using synchrotron radiation from the 2.5 GeV storage ring. A white X-ray beam was monochromatized by a Si(111) double-crystal monochromator with detuning to 60% in intensity to eliminate the harmonics. The intensity of the incident and transmitted X-ray beams were measured in ionization chambers filled with nitrogen gas.

## 3. Results and discussion

### 3.1. Phase diagrams

Fig. 2 is the phase diagram of $LiMn_2O_4$ in the temperature–oxygen partial pressure system ($T$–$P_{O2}$) obtained by TG/DTA analysis [10]. The metastable samples of high-temperature phases were obtained by quenching from the corresponding temperatures in the regions B and C in Fig. 2. The sample was quickly taken from the furnace and dropped into liquid nitrogen. The X-ray diffraction study for samples quenched from various temperatures revealed that line 1 in Fig. 2 represents the onset of oxygen extraction and line 2 corresponds to the formation of orthorhombic $LiMnO_2$ (Pmnm). Oxygen extraction in region B via complicated processes leads to the formation of a tetragonal spinel with the nominal composition $LiMn_2O_{3.86}$ ($I4_1/amd$, $c/a = 1.07$) [18]. However, the defect structure models for the oxygen released metastable phase are still controversial [18,19].

It should be noted, for either lithium insertion [13] or oxygen extraction [10,14,15], that quite a small perturbation reduces the manganese valence and immediately induces the JT distortion. Fig. 3 shows the suppression of JT distortion by dilution with non-JT ions, $Mn^{2+}$ and $Mn^{4+}$, at room temperature [10–12]. The important point is that

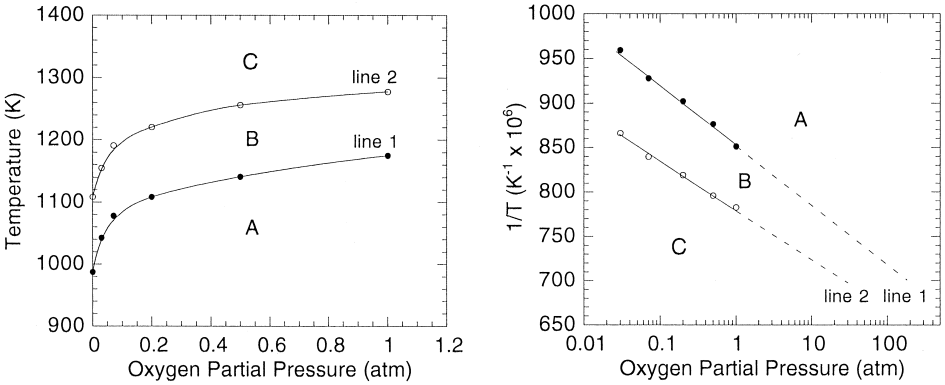


Fig. 2. Phase diagram of $LiMn_2O_4$ in the temperature–oxygen partial pressure system.

$LiMn_2O_4$ is positioned on the boundary between the cubic and the tetragonal phases, thus, $LiMn_2O_4$ is apt to exhibit JT distortion with only a slight increase of $Mn^{3+}$. Considering the position of $LiMn_2O_4$ in the phase diagram, we speculated that low temperature JT transitions occur when the temperature change enhances cooperative JT interaction. In order to test the validity of this speculation, low temperature thermal analysis and X-ray diffraction studies were performed [11].

### 3.2. Temperature-induced JT transition

As shown in Figs. 4 and 5, both DSC and X-ray diffraction data clearly show a first-order transition at $T_t \sim 280$ K from Fd3m ($T > T_t$) to $I4_1/amd$ ($T < T_t$) with a temperature hysteresis of ca. 10 K [11]. The thermal expansion and its temperature coefficient also showed a discontinuous, stepwise anomaly at $T_t$ [11]. This transition is induced by the weak and almost undetectable JT effect of $Mn^{3+}$ in the mixed valence state with JT inactive $Mn^{4+}$ ions [9]. The cubic phase remained stable below $T_t$, however, with up to ca. 35% in volume, and the tetragonal distortion was as small as $c/a = 1.011$ [11] (Fig. 6). These values were obtained from the separation of the diffraction peak at (440), assuming that the low-temperature phase is a mixture of the cubic Fd3m and tetragonal $I4_1/amd$ phases. The single tetragonal phase does not appear until 8 K [20]. This stable phase segregation may come from a charge-ordered state, that is, a formation of $Li^+$-rich ($Mn^{3+}$-rich) and $Li^+$-poor ($Mn^{4+}$-rich) regions, as indicated by $Li^7$ NMR [21] and resistivity data [22].

After our first report of the transition in 1995 [11], various physical properties, e.g., the elastic constant [23], electronic conductivity [22], magnetic susceptibility [22], and the infrared absorption spectra [24], were investigated in the vicinity of $T_t$ and were found to show a clear anomaly at $T_t$. It should be noted that highly sophisticated structural analysis of material in the low temperature phase is recently performed by Oikawa et al. [25], Hayakawa et al. [33], and Rousse et al. [34] using Rietvelt analysis of neutron and X-ray diffraction patterns. They concluded the low-temperature phase to be single phase orthorhombic instead of the cubic–tetragonal mixture and observed su-

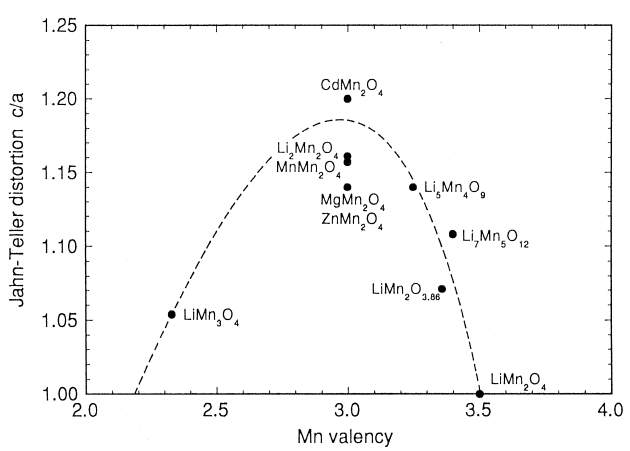


Fig. 3. The suppression of the JT effect of $Mn^{3+}$ by non-JT ions, $Mn^{2+}$ and $Mn^{4+}$.

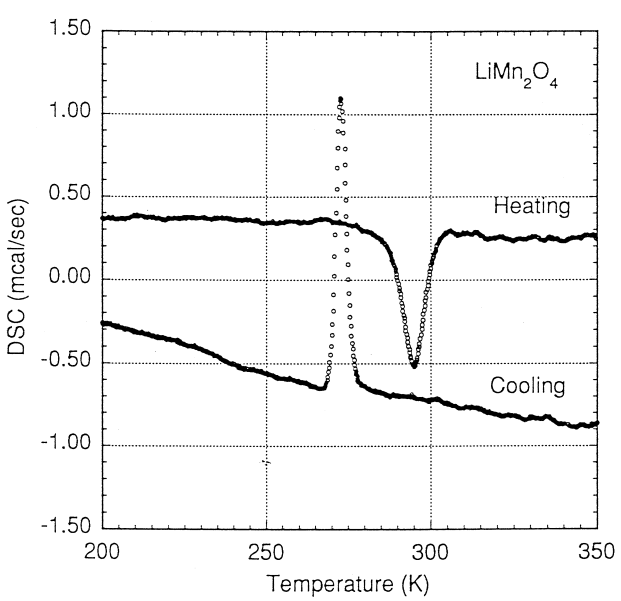


Fig. 4. DSC trace for $LiMn_2O_4$.

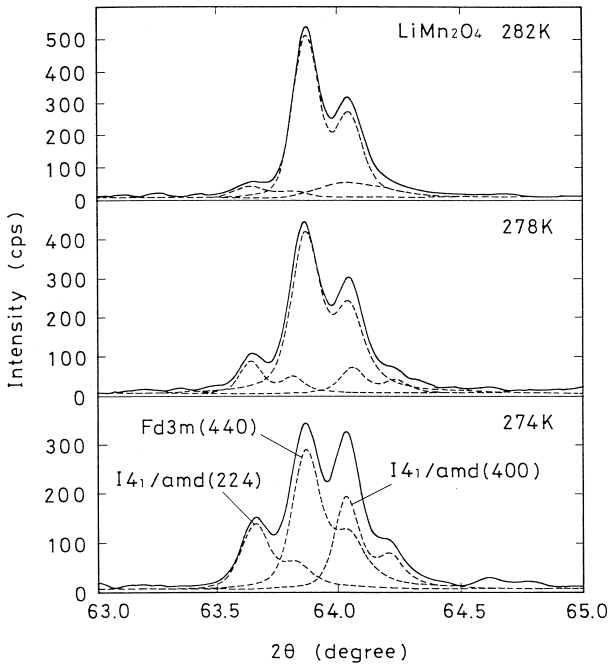


Fig. 5. Peak separation analysis of the superimposed peak of Fd3m (440), $I4_1/amd$ (224), and $I4_1/amd$ (400) in X-ray diffraction data.

perlattice reflections with tripled periodicity in the electron diffraction patterns. The superlattice reflections were indexed by the $3a \times 3a \times c$ supercell with partial charge ordering [34]. Further studies are required to elucidate the detailed mechanism of the transition.

The usual way to suppress JT instability in $LiMn_2O_4$ and to improve the cycling performance of a battery cathode is to substitute 1–2% of Mn with another element to form $Li(A_{-}Mn_{2-x})O_4$, which causes a reduction of the concentration of octahedral-site $Mn^{3+}$ ions per formula unit. Much work has been done on the cathode performance of $Li(A_xMn_{2-x})O_4$ [26]. However, there has always been a trade-off between cycling performance and rechargeable capacity. The origin of the reduction in capacity can be quantitatively accounted for as a simple function of the initial manganese valence.

Conversely, there has been no direct, quantitative measure of JT instability in the system $Li(A_xMn_{2-x})O_4$ with the goal of improving cycling performance. Although it is well known that the Mn16d site in $LiMn_2O_4$ accepts some elements for substitution, we have chosen Li-substituted spinel $Li(Li_xMn_{2-x})O_4$ [6,27] as a model system for a quantitative evaluation of JT instability with respect to the phase transition at 280 K [16]. Our choice was based on two technical considerations: (1) A small amount of substitution is effective with minimal influence on the randomness because of the monovalent $Li^+$, and (2) $Li^+$ is a lightweight, inexpensive element easily substituted for Mn(16d) in $LiMn_2O_4$ [16].

As shown in Fig. 7, the phase transition temperature, $T_t$, as given by the DSC peak position in the heating process, dramatically decreases from 282.3 to 214.3 K when a very small amount of Mn is replaced by Li ($x < 0.033$). At the same time, the latent heat $\Delta H$ is suppressed from 271.0 cal/mol to 28.9 cal/mol. Finally, the transition disappears at around $x = 0.035$, which corresponds to merely $< 2\%$ Li substitution of Mn. A similar phenomenon has been reported in other $LiMn_2O_4$-based materials which have a Mn valence larger than 3.5, e.g., defect-type spinels, $Li_{1-x}Mn_{2-2x}O_4$ [28].

The JT transition just below room temperature ($T_t \sim 280$ K) proves that spinel $LiMn_2O_4$ inherently involves large JT instability. The lower transition temperature and the smaller latent heat in $Li(Li_xMn_{2-x})O_4$ indicate that charge-compensating holes occupy the Mn3d $e_g$ band to increase Mn valency and stabilize the cubic phase. The measurement of the transition temperature $T_t$ and the latent heat $\Delta H$ derived from thermal analysis is straightforward, and these parameters are very sensitive to the composition. Thus, this phenomenon provides a simple yet powerful

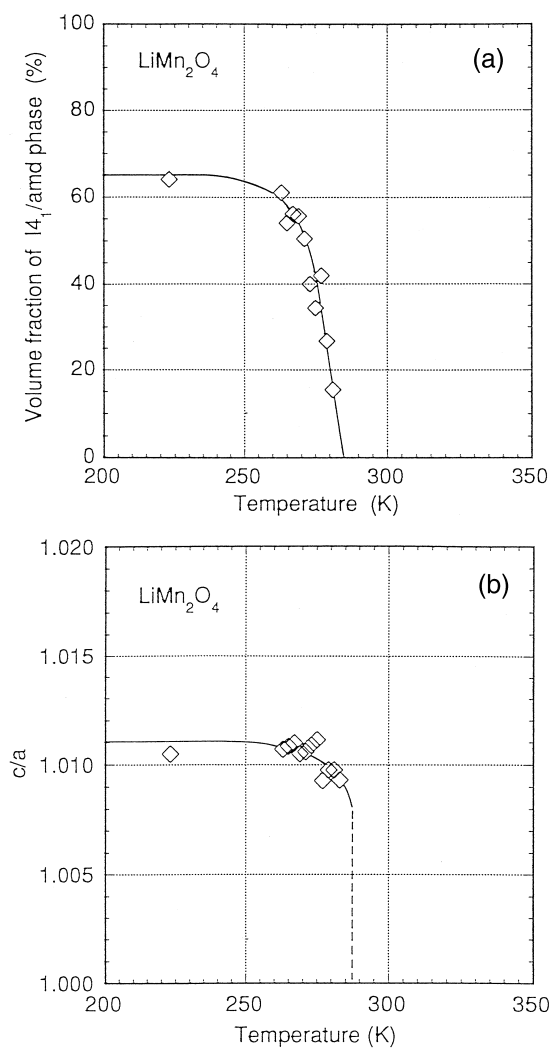


Fig. 6. The temperature dependence of (a) the volume fraction of the tetragonal phase and (b) the lattice distortion $c/a$ in $LiMn_2O_4$.

technique for quantitative estimation of JT instability for materials design.

### 3.3. Local distortion around $Mn^{3+}$

Thus far, we have discussed JT instability based on the average crystallographic structure. However, regardless of where the redox process is within the $Mn^{4+/3+}$ couple, each $(Mn^{3+}O_6)^{9-}$ octahedron is locally influenced by the JT effect even if the average structure is cubic. This occurs because lithium manganese oxides are small polaron conductors [29] where hopping electrons are localized within the time scale corresponding to the period of the optical vibration mode which traps them in a local potential well. In this situation, the microscopic rearrangement of the local structure, which cannot be detected in average crystallographic data, may affect battery performance. Therefore, thorough investigation of JT instability, using both macroscopic and microscopic techniques, is necessary.

Indeed, there are many reports that local structure is quite distinct from that suggested by the average crystallographic structure of a mixed valence transition metal oxide, where polarons link with the specific mode of the optical phonon. A direct link between the JT distortions and the polaron is possible in analogy with the case of $(La_{1-x}Sr_x)MnO_3$ perovskite; local JT distortion as large as that in $LaMnO_3$ was evident even in the wide rhombohedral phase ($x > 0.16$) not only from EXAFS data but also from pair-density-function (PDF) analysis of pulsed neutron diffraction data [30–32].

Accordingly, we tried to identify similar local JT distortion in $LiMn_2O_4$ ($Mn^{3.5+}$, cubic Fd3m) by an EXAFS study using $ZnMn_2O_4$ ($Mn^{3+}$, tetragonal $14_1/amd$) and λ-$MnO_2$ as reference samples, all have different valence states but maintain the framework of the spinel structure. Details of the experimental data and their analysis are now being summarized and will be reported elsewhere [17]. Here, we briefly mention the results.

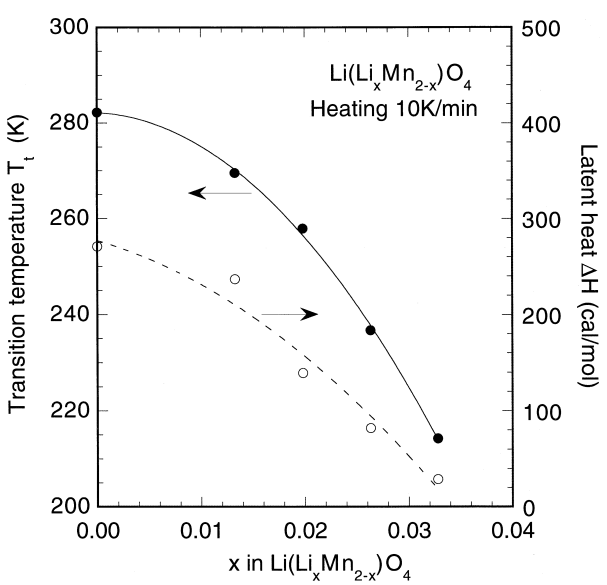


Fig. 7. The change in the phase transition temperature $T_t$ and the latent heat $\Delta H$ as a function of Li substitution $x$ in $Li(Li_xMn_{2-x})O_4$.

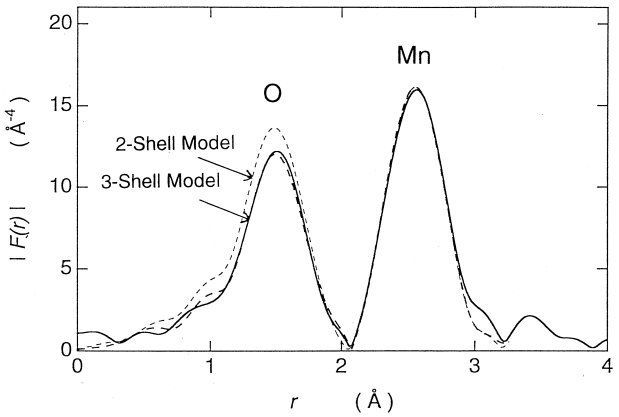


Fig. 8. Radial distribution around Mn in $LiMn_2O_4$ obtained by Mn K-edge EXAFS. Solid line: experimental data, thin dashed line: calculated values fitted to the two-shell model, thick dashed line: fitted to the three-shell model [17].

For λ-$MnO_2$ and $ZnMn_2O_4$, local structure models consistent with the crystallographic spinel structure were quite effective for fitting, where the residual factor R was as small as 0.07–0.09. On the other hand, for $LiMn_2O_4$ it was found that structural parameters based on X-ray diffraction data (the '2-shell model' with six oxygen ions at the nearest neighbor and six manganese ions at the second nearest sites) did not reproduce the damping observed in EXAFS ($R = 0.12$). The fitting was significantly improved to $R = 0.06$, which is as small as that of the reference samples, by using the local distortion model (the '3-shell model' with one long Mn–O, five short Mn–O, and one Mn–Mn) assuming the cubic $Mn^{4+}O_6$ octahedra and the distorted $Mn^{3+}O_6$ octahedra with $c/a = 1.17$, as shown in Fig. 8. It should be noted that the magnitude of the local distortion is as large as that of tetragonal $ZnMn_2O_4$.

Thus, it is most likely that large JT distortion ($c/a = 1.17$) is locally present around $Mn^{3+}$, even in cubic $LiMn_2O_4$ and that the magnitude of JT distortion is unchanged by introducing $Mn^{4+}$. This is clearly seen in the $La_{1-x}Sr_xMnO_3$ perovskite system, where the orientation of local JT distortion varies from site to site where the cubic symmetry is only maintained as an average.

## 4. Conclusion

The discovery of the JT transition just below room temperature ($T_t \sim 280$ K) demonstrated that spinel $LiMn_2O_4$ inherently involves large JT instability. Sensitive parameters, $T_t$ and $\Delta H$, were provided for quantitative estimation of JT instability in the practical composition

region in the spinel Li–Mn–O ternary system. The EXAFS analysis showed a significant large local JT distortion ($c/a = 1.17$) around $Mn^{3+}$ even in cubic $LiMn_2O_4$. Further investigations of this issue are now in progress.

## Acknowledgements

The authors are grateful to Prof. J.B. Goodenough and Dr. J.S. Zhou for informative discussions, and Prof. H. Uwe and Dr. H. Yamaguchi for their cooperation in the EXAFS study.

## References

[1] M.M. Thackeray, P.J. Johnson, L.A. de Picciotto, P.G. Bruce, J.B. Goodenough, Mater. Res. Bull. 19 (1984) 179.
[2] T. Ohzuku, A. Ueda, T. Hirai, Chem. Express. 7 (1992) 193.
[3] A.R. Armstrong, P.G. Bruce, Nature 381 (1996) 499.
[4] A.R. Armstrong, R. Gitzendanner, A.D. Robertson, P.G. Bruce, J.C.S. Chem. Commun. 1998 (1998) 1833.
[5] J. Kim, A. Manthiram, Nature 390 (1997) 265.
[6] R.J. Gummow, A. de Kock, M.M. Thackeray, Solid State Ionics 69 (1994) 59.
[7] M.M. Thackeray, Y.S. Horn, A.J. Kahaian, K.D. Kepler, E. Skinner, J.T. Vaughey, S.A. Hackney, Electrochem. Solid State Lett. 1 (1998) 7.
[8] J.B. Goodenough, Magnetism and the Chemical Bond, Wiley, New York (1963).
[9] A. Yamada, M. Tanaka, K. Tanaka, 8th International Meetings on Lithium Batteries (IMLB-8), Extended Abstracts, II-B-46 (1996) 496.
[10] A. Yamada, K. Miura, K. Hinokuma, M. Tanaka, J. Electrochem. Soc. 142 (1995) 2149.
[11] A. Yamada, M. Tanaka, Mater. Res. Bull. 30 (1995) 715.
[12] K. Miura, A. Yamada, M. Tanaka, Electrochim. Acta 41 (1996) 249.
[13] T. Ohzuku, N. Kitagawa, T. Hirai, J. Electrochem. Soc. 137 (1990) 769.
[14] J.M. Tarascon, W.R. McKinnon, F. Coowar, T.N. Bowmer, G. Amatucci, D. Guyomard, J. Electrochem. Soc. 141 (1994) 1421.
[15] J. Sugiyama, T. Atsumi, T. Hioki, S. Noda, N. Kamegashira, J. Alloys and Comp. 235 (1996) 163.
[16] A. Yamada, J. Solid State Chem. 122 (1996) 160.
[17] H. Yamaguchi, A. Yamada, H. Uwe, Phys. Rev. B 58 (1998) 8.
[18] M.M. Thackeray, M.F. Mansuetto, D.W. Dees, D.R. Vissers, Mater. Res. Bull. 31 (1996) 133.
[19] M. Hosoya, H. Ikuta, T. Uchida, M. Wakihara, J. Electrochem. Soc. 144 (1997) L52.
[20] M. Wakihara, L. Guohua, H. Ikuta, Lithium Ion Batteries, in: M. Wakihara, O. Yamamoto (Eds.), Chap. 2, Kodansha, 1998.
[21] A. Koiwai, J. Sugiyama, T. Hioki, S. Noda, J. Power Sources 68 (1997) 637.
[22] Y. Shimakawa, T. Murata, J. Tabuchi, J. Solid State Chem. 131 (1997) 138.
[23] J. Sugiyama, T. Tamura, H. Yamauchi, J. Phys.: Condens. Matter 7 (1995) 9755.
[24] K.A. Striebel, S.J. Wen, E.J. Cairns, Abstract 828, The Electrochemical Society Meeting Abstracts, Vol. 96-2, San Antonio, TX, Oct. 6–11, 1996, p. 1016.
[25] K. Oikawa, T. Kamiyama, F. Izumi, B.C. Chakoumakos, H. Ikuta, M. Wakihara, J. Li, Y. Matsui, Solid State Ionics 109 (1998) 35.
[26] L. Guohua, H. Ikuta, T. Uchida, M. Wakihara, J. Electrochem. Soc. 143 (1996) 178.
[27] Y. Gao, J.N. Reimers, J.R. Dahn, Phys. Rev. B 54 (1996) 3878.
[28] C. Masquelier, M. Tabuchi, K. Ado, R.J. Kanno, Y. Kobayashi, Y. Maki, O. Nakamura, J.B. Goodenough, J. Solid State Chem. 123 (1996) 255.
[29] J.B. Goodenough, Lithium Ion Batteries, in: M. Wakihara, O. Yamamoto (Eds.), Chap. 1, Kodansha, 1998.
[30] T.A. Tyson, J.M. de Leon, S.D. Conradson, A.R. Bishop, J.J. Neumeier, H. Roder, J. Zang, Phys. Rev. B 53 (1996) 13985.
[31] G.H. Booth, F. Bridges, G.J. Snyder, T.H. Geballe, Phys. Rev. B 54 (1996) 15606.
[32] D. Louca, T. Egami, E.L. Brosha, H. Roder, A.R. Bishop, Phys. Rev. B 56 (1997) 8475.
[33] H. Hayakawa, T. Takada, H. Enoki, E. Akiba, J. Mater. Sci. Lett. 17 (1998) 811.
[34] G. Rousse, C. Masquelier, J. Rodriguez-Carvajal, M. Hervieu, Electrochem. Solid State Lett. 2 (1999) 6.